The Effect of Grit Blasting on the Oxidation Behavior of a Platinum-Modified Nickel-Aluminide Coating

V.K. TOLPYGO, D.R. CLARKE, and K.S. MURPHY

The surface of platinum-modified nickel-aluminide bond coats on superalloys is usually roughened by grit blasting prior to deposition of thermal barrier coatings (TBCs). Analysis of the grit-blasted surface by secondary ion mass spectrometry (SIMS) reveals that this pretreatment leads to contamination of the bond coat by various impurities, in particular, the alkali and alkaline-earth metals and titanium. These impurities then become incorporated into the growing alumina scale and adversely affect the oxidation behavior of the bond coat. In particular, it is shown that grit blasting results in about a tenfold increase of the oxidation rate and extensive scale spallation during cyclic oxidation at 1150 °C.

I. INTRODUCTION

COMMERCIAL thermal barrier coatings (TBCs) applied on the surface of turbine superalloys consist of an yttria-stabilized zirconia (YSZ) ceramic coating and an aluminum-rich metallic bond coat. The bond coat provides oxidation protection for the underlying superalloy by forming an adherent and slowly growing α-Al_2O_3 oxide scale. The platinum-modified nickel-aluminide, β-(Ni,Pt)Al, is among the most oxidation-resistant bond coats. It is deposited by platinum electroplating followed by a low-Al-activity chemical vapor deposition (CVD) process.[1] A number of studies have been focused on the oxidation behavior of such coatings, in particular with respect to the role of surface imperfections (grain-boundary ridges)[2] and sulfur impurities in the bond coat.[3,4,5]

Extensive literature on the oxidation of high-temperature alloys, which has developed in recent years, shows that decreasing the sulfur content in the alloys dramatically increases the time at temperature before failure of the protective oxide occurs.[6,7] The beneficial effect of decreasing the sulfur content is also expected in the bond coats in TBC systems; therefore, considerable effort has been devoted to developing low-sulfur alloys and a "clean" CVD process for low-sulfur aluminide coatings.[1]

The focus on sulfur as the major detrimental impurity has, perhaps, diverted attention from other impurities, especially ones that may be introduced into the alloy surface in the variety of postcasting treatments. One of the most common manufacturing treatments is grit blasting (sand blasting). This is used, for instance, to remove mold debris from cast components, to prepare a component prior to the application of a bond coat, as well as to prepare a bond-coat surface before deposition of a TBC. In the latter case, grit blasting is believed to be necessary to ensure mechanical bonding of the top YSZ coating with the bond-coat surface and to provide standard surface conditions for TBC application. Besides, this pretreatment was found to promote the formation of the alpha-alumina oxide at the intermediate-temperature range,[8] where nickel aluminides tend to form metastable alumina polymorphs. However, the long-term effect of grit blasting on the protective properties of alumina scales has not been reported so far.

In this work, we describe the effect of grit blasting on the oxidation behavior of a (Ni,Pt)Al bond coat. It will be shown that impurities are introduced into the bond-coat surface by grit blasting and that these impurities are subsequently incorporated into the thermally grown oxide formed on oxidation. Furthermore, it is found that impurity incorporation in the growing oxide results in a dramatic increase in the oxidation rate, adversely affects its microstructure, and increases its susceptibility to failure by spalling. Although the impurity content will undoubtedly vary from one grit-blasting medium to another and, indeed, probably from one batch to another, the central findings of the work presented here will be the same. Apart from the significance of these findings for guiding improvements in alloy processing, they are also of importance in demonstrating that cation impurities can greatly influence the development and growth rate of alpha-alumina scales on high-temperature alloys.

II. EXPERIMENTAL DETAILS

The samples studied were bond-coated disks (25.4 mm in diameter and 3-mm thick) of the single-crystal superalloy with a nominal composition of Ni-7.5Co-7Cr-6.5Ta-6.2Al-5W-3Re-1.5Mo-0.15Hf-0.01Y (wt pct), provided by Howmet Corporation. The low-Al-activity platinum-modified CVD coating was deposited on all sides of the disks. A number of the samples were examined in their as-aluminized condition. In the following text, these samples will be referred to as samples A. The other samples (designated B) were grit blasted with fine corundum particles (−220 grit Al_2O_3) using standard commercial equipment. According to the alumina certification data, it contained TiO_2 (about 3 wt pct), SiO_2, CaO, MgO (less than 0.1 wt pct of each), and other common impurities, which is typical to commercial alumina used throughout the coating industry.

The bond coat consisted of an outer layer of β-(Ni,Pt)Al (about 35-μm thick) and an inner multiphase diffusion zone

V.K. TOLPYGO, Assistant Researcher, and D.R. CLARKE, Professor, are with the Materials Department, University of California, Santa Barbara, CA 93106. K.S. MURPHY, Senior Project Engineer, is with Howmet Research Corporation, Whitehall, MI 49461.

Manuscript submitted August 10, 2000.

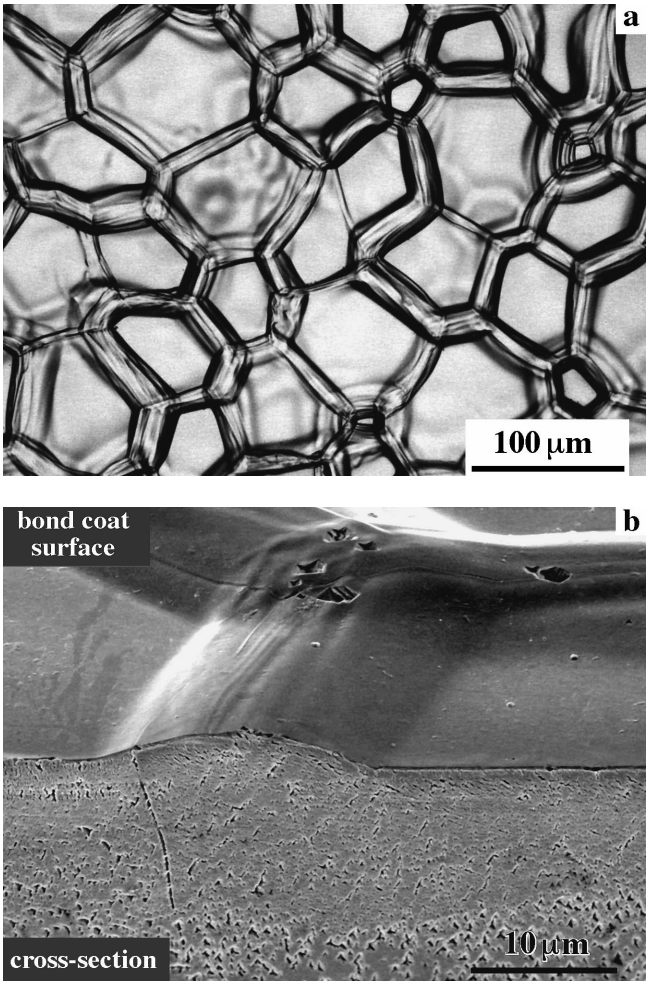

Fig. 1—The microstructure of the as-aluminized (Ni,Pt)Al bond coat: (*a*) optical micrograph showing ridges along grain boundaries and (*b*) SEM image showing the etched cross section and surface of the bond coat.

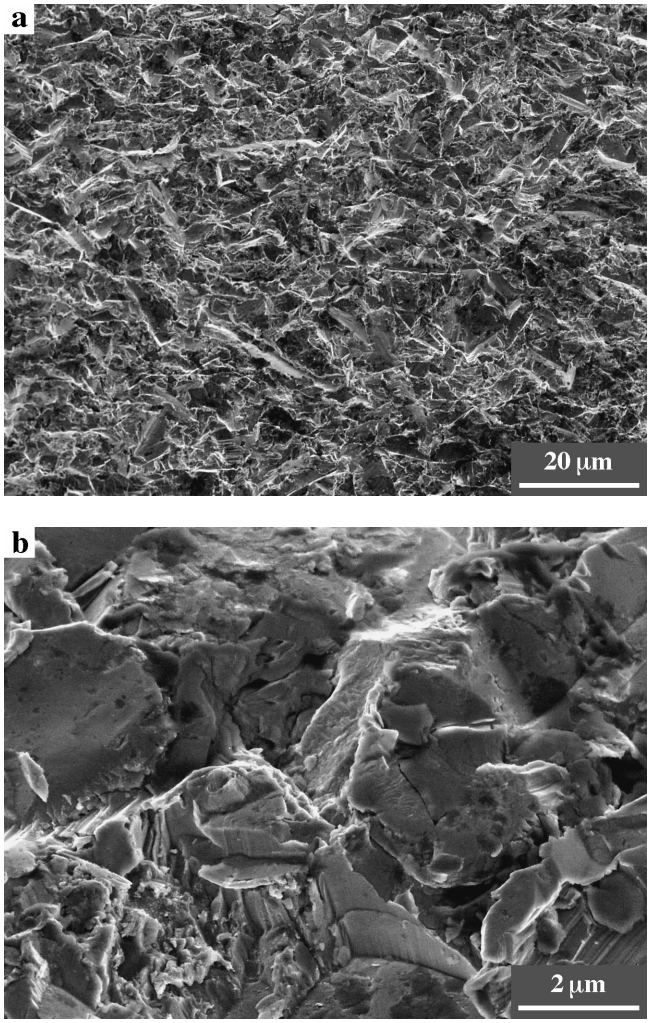

Fig. 2—Microstructure of the grit-blasted surface of the bond coat: (*a*) low-magnification micrograph and (*b*) higher-magnification view showing the surface damage produced by grit blasting.

(about 30-μm thick). The approximate chemical composition of the coating surface, determined by X-ray energy dispersive spectroscopy (EDS), was as follows (at. pct): 45Ni-44Al-6Pt-3.5Co-1.5Cr. The microstructure of the bond coat prior to oxidation is shown in Figures 1 and 2. In the as-aluminized condition (Figure 1), the coating surface is rather smooth, with distinct ridges along grain boundaries of the β layer and flat regions between the ridges. Grit blasting produces a very rough surface with numerous sharp edges, craters, and microcracks, whereas the grain-boundary ridges become barely discernible (Figure 2). All samples were degreased, rinsed in water, and ultrasonically cleaned in ethanol and acetone prior to oxidation.

The samples were cyclically oxidized at 1150 °C in static air. Each cycle consisted of 10 hours of exposure at 1150 °C, with heating and cooling rates of about 200 °C/min. Such a high oxidation temperature was chosen in order to develop an alpha-alumina scale from the beginning of oxidation and to avoid possible effects related to the formation of other metastable oxides and their transformation into the stable α phase.

The surface of the bond coat after oxidation was characterized by optical and scanning electron microscopy (SEM), and the oxidation kinetics was monitored by measuring the mass change at room temperature after each second cycle (the mass of spalled oxide fragments was not included). The distribution of various elements across the subsurface region of the bond-coat surface prior to oxidation, as well as through the alumina scale thickness after 10 hours of oxidation at 1150 °C, was studied by secondary ion mass spectrometry (SIMS). Several mass spectra were first recorded from different areas for identification of the major impurities. Then, standard depth profiling of selected elements was performed over an area of about 100 × 100 μm^2 (the sputtered area was 0.3 × 0.3 mm^2) and up to 2 to 3 μm in depth. Most elements, in the form of positive ions, were analyzed by a quadrupole system with an oxygen primary beam operating at 8 keV. In some cases, a Cs^+ beam was used for nonmetallic elements (analyzed as negative ions). Because of the mass interference of all sulfur isotopes with oxygen ions, sulfur could not be analyzed in this work.

III. RESULTS

A. *Oxidation Kinetics*

Figure 3(a) presents the mass changes in the course of cyclic oxidation at 1150 °C of two bond-coated samples.

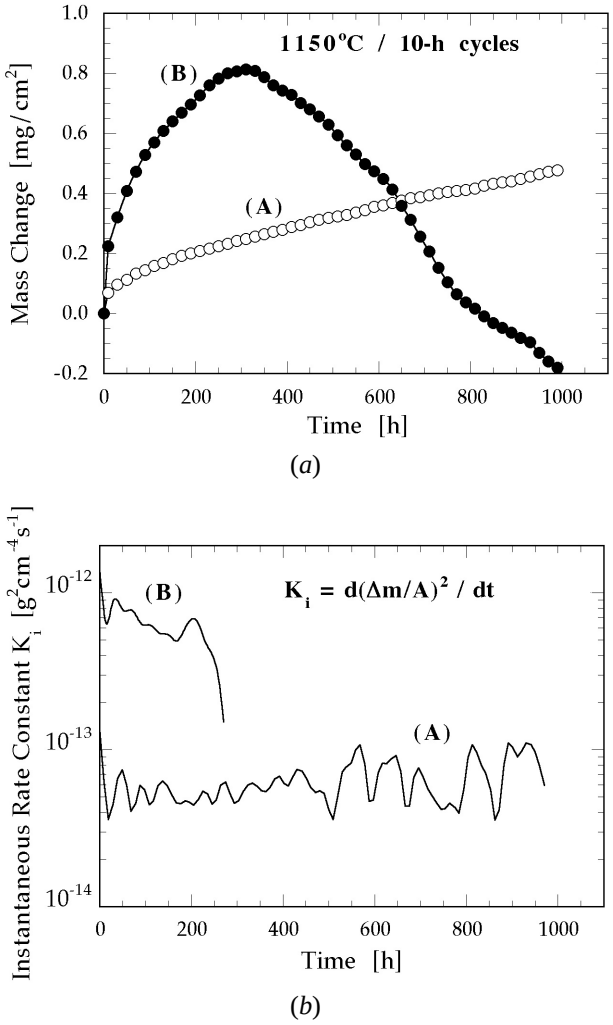

Fig. 3—Kinetics of cyclic oxidation of the as-aluminized (A) and grit-blasted (B) samples at 1150 °C (10-h cycles): (*a*) mass change and (*b*) instantaneous oxidation rate constant as a function of time.

Both the as-aluminized (A) and grit-blasted (B) samples form α-Al_2O_3 scale (which was confirmed by photoluminescence); however, their oxidation behavior is notably different. The oxide formed on the grit-blasted surface exhibits a much higher growth rate. In addition, extensive spallation of the scale occurred on this sample as early as after 10 to 15 cycles and subsequently resulted in a mass decrease after about 30 cycles (300 hours total time at 1150 °C). In contrast, no spallation was observed on sample A, except for a few localized places, and its mass-change curve in Figure 3(a) exhibits a steady increase during oxidation for up to 1000 hours. Based on the mass-gain data, the scale thickness on the as-aluminized sample is about 2.5 μm after oxidation for 1000 hours, whereas on the grit-blasted sample, the same thickness is attained after only 60 hours.

In order to qualitatively compare the oxidation kinetics of the grit-blasted and as-aluminized samples, the "instantaneous" rate constants, calculated as $K_i = d(\Delta m/A)^2/dt$, where $\Delta m/A$ is the mass gain per unit area and t is time, are presented in Figure 3(b). The formation of a highly adherent scale on sample A justifies the use of the oxidation rate constant for cyclic tests within the time interval studied. The rate constant for sample B is included in Figure 3(b) for the initial period of about 250 hours, prior to significant spalling. Although neither of the oxidation kinetics is strictly parabolic (since the K_i values are not constant), the comparison shows that oxidation of the grit-blasted bond coat occurs about 10 times faster than oxidation of the as-aluminized bond coat, and the average rate constants are, respectively, $6 \cdot 10^{-13}$ g^2 cm^{-4} s^{-1} and $6 \cdot 10^{-14}$ g^2 cm^{-4} s^{-1}.

B. *SIMS Analysis of Impurities*

The as-aluminized and grit-blasted samples were analyzed by SIMS prior to oxidation, in order to determine impurities that were present on the bond-coat surface. Figure 4 shows the depth profiles of some of the impurities together with the two major constituents, Ni and Cr. The distance from the coating surface, indicated on the top axis of each plot, was estimated by measuring the depth of the sputtered crater.

Although the results are not quantified in terms of impurity concentration (which would require reliable standards), the difference between the two samples is, nonetheless, striking. In both cases, an increased content of alkali and alkaline-earth elements is observed at the bond-coat surface; however, the enrichment is much stronger and extends far deeper into the bulk material after grit blasting (Figure 4(b)). There is also a significant increase of Ti content on the grit-blasted surface, but not on the as-aluminized surface. The depth profiles of the major element, Ni, in Figures 4(a) and (b) are very similar. This indicates that both samples were analyzed in identical conditions and, therefore, the profiles of the other elements can be directly compared. Some other impurities—Fe, Si, Ba, F, P, and Cl (the last three were analyzed as negative ions)—although not included here, were also detected at the bond-coat surface. Similar to the elements shown in Figure 4, their content was higher in the grit-blasted sample than in the as-aluminized sample. Other major components in the coating (Al, Pt and Co) did not exhibit any significant difference between the grit-blasted and as-aluminized samples. Finally, the refractory metals (Mo, Ta, *etc.*) were not analyzed, as their ion yields were near the detection limit of SIMS.

Since all the elements shown in Figure 4 have different ionization efficiencies, no quantitative comparison between their concentrations can be made. Nevertheless, assuming that the ionization efficiency of Na, Ca, and K is, for instance, about 10 to 20 times higher than that of Cr,[9] it appears that the content of these elements on the grit-blasted surface is only one order of magnitude smaller than chromium, *i.e.*, of the order of 0.1 at. pct.

A better comparison between the two samples can be made using the ratio of secondary-ion counts for each element as a function of sputtering time. Since the rate of sputtering was approximately the same for both samples, this ratio clearly demonstrates the difference in impurity distributions across the subsurface region. Figure 5 shows that the content of alkali and alkaline-earth elements (Li, Na, Mg, K, Ca, and Sr) and titanium is 10 to 1000 times higher on the grit-blasted surface. In contrast, the ratios for Ni and Cr are very close to 1, justifying the direct comparison between the samples and also indicating that the roughness (and, correspondingly, larger surface area) of the grit-blasted surface has only a minor effect on the SIMS signal.

Figure 6 presents the SIMS depth profiles obtained on the same two samples as in Figures 4 and 5, but after one

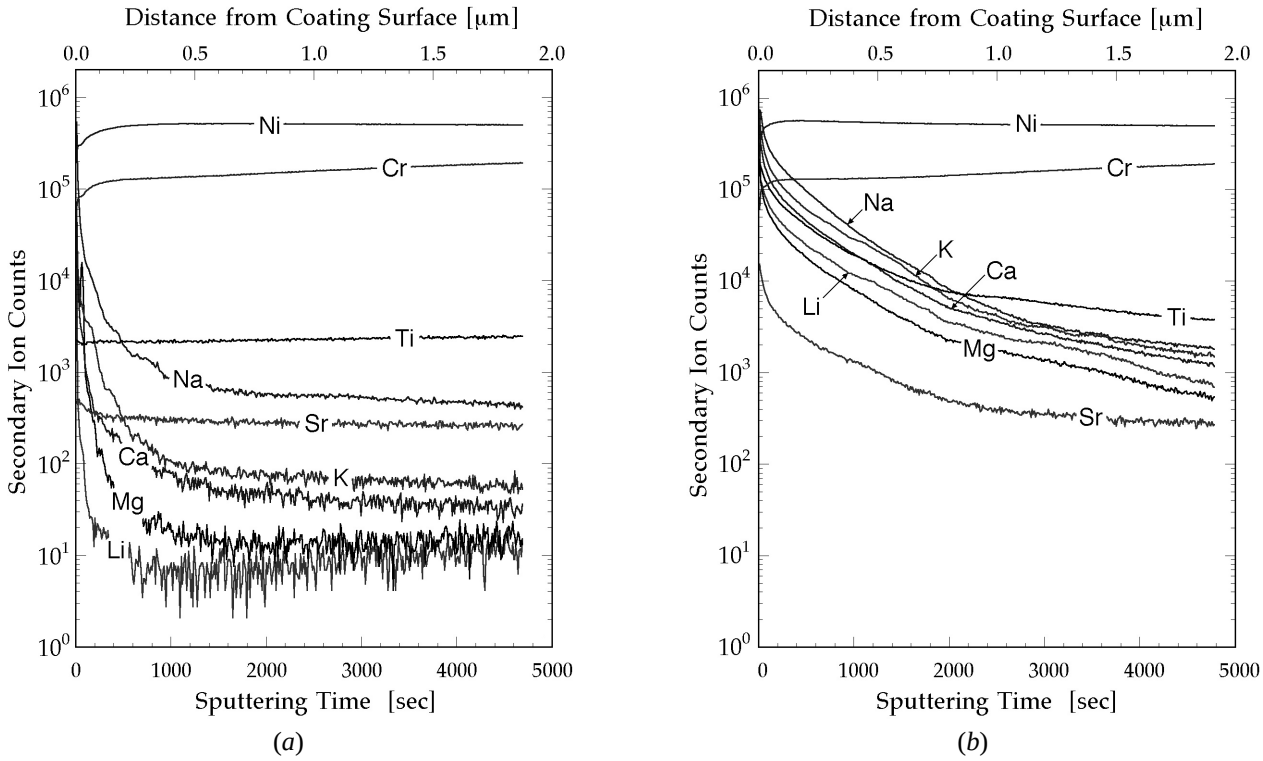

Fig. 4—SIMS depth profiles of selected elements through the (*a*) as-aluminized and (*b*) grit-blasted bond coats before oxidation.

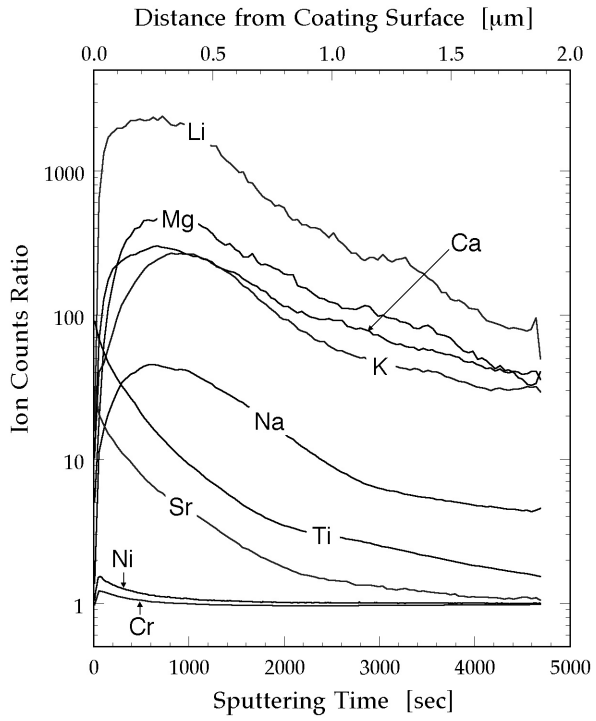

Fig. 5—Ion intensity ratio (grit-blasted/as-aluminized) calculated using the depth profiles before oxidation in Fig. 4. The ratio shows the actual difference in impurity concentration near the bond coat surface between the two samples.

oxidation cycle (10 hours) at 1150 °C in air. In both cases, the measurements were performed through the entire oxide thickness. The depth resolution in these measurements is rather poor, because of the surface roughness (which results in nonuniform sputtering), oxide thickness variations, and the large size of the analyzed area. For this reason, only an approximate position of the oxide-metal interface can be indicated. It is marked in Figure 6 as a shaded region, across which Ni and Cr counts increase and Al counts decrease. The elements in Figure 6 are divided into two groups in order to better resolve individual profiles. As mentioned previously, sulfur could not be accurately analyzed by SIMS; therefore, it is not included among the impurities presented in Figures 4 through 6.

The most striking result of the SIMS analysis of the oxidized samples is that all the impurities detected on the bond-coat surface prior to oxidation become incorporated into the α-Al_2O_3 scale. Similar to the depth profiles before oxidation (Figure 4), the content of all impurities in the scale is significantly higher in the oxide formed on the grit-blasted bond coat. Since the sputter rate is not constant during depth profiling through the oxide layer and then through the metal, the distance from the surface is not indicated in Figure 6. Based on the mass-gain data in Figure 3, the estimated oxide thickness after oxidation for 10 hours is about 0.3 μm on the as-aluminized sample and 1.1 μm on the grit-blasted sample.

In Figure 7, the depth profiles of the major impurities from Figure 6 are presented in the form of relative SIMS intensities ($M^+/^{27}Al^+$, where M^+ represents $^7Li^+$, $^{23}Na^+$, $^{40}Ca^+$, *etc.*), which provides a rough estimate of the impurity concentration in alumina. If the relative intensity of magnesium ($^{24}Mg^+/^{27}Al^+$) is assumed to be very close to the atomic ratio Mg/Al,[10] then, for example, at $^{24}Mg^+/^{27}Al^+ = 10^{-3}$, the estimated content of magnesium in Al_2O_3 is about 1000 times smaller than that of aluminum, *i.e.*, of the order of 400 ppma. Similar estimates are probably valid for other

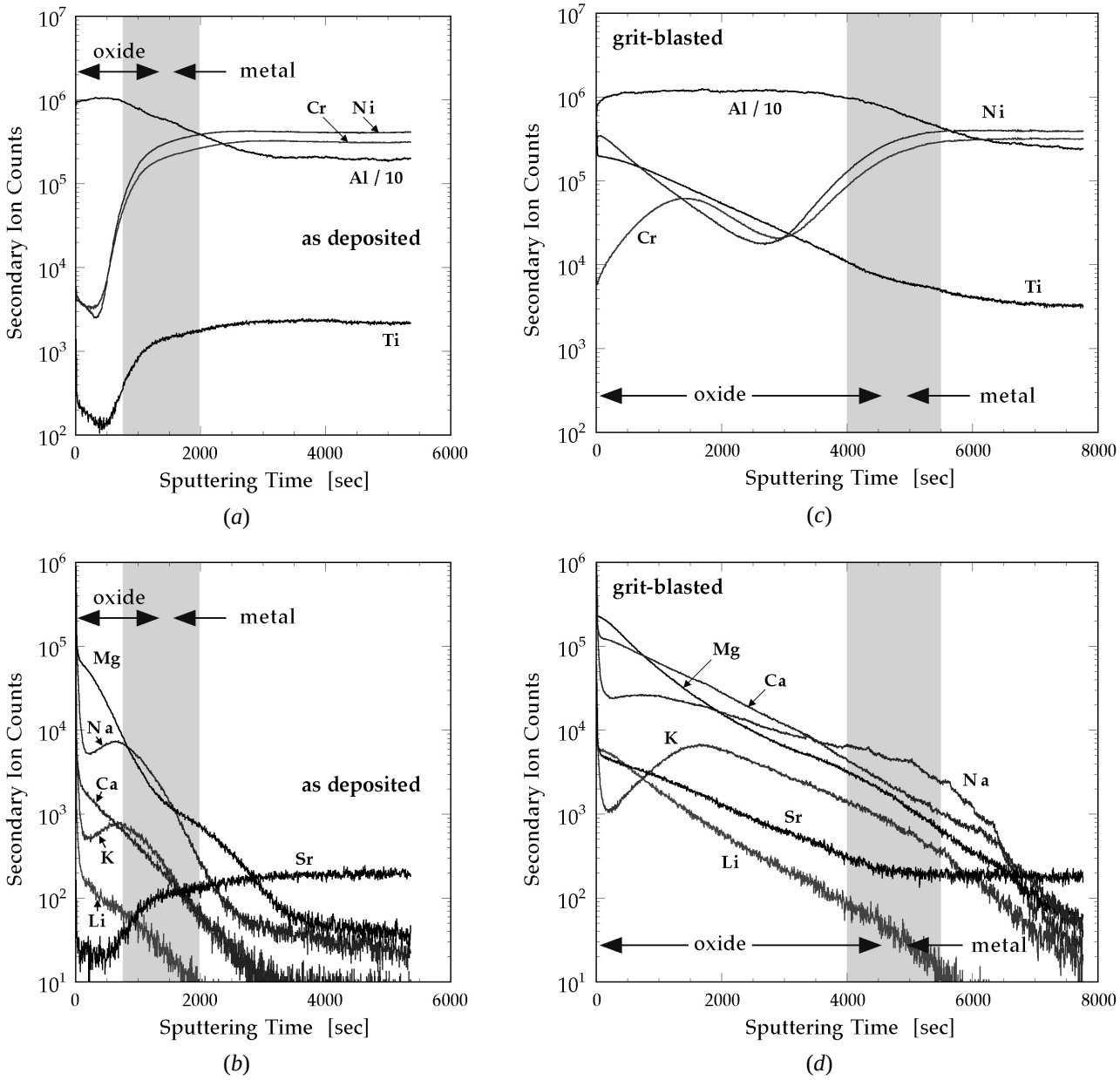

Fig. 6—SIMS depth profiles through the (*a*) and (*b*) as-aluminized and (*c*) and (*d*) grit-blasted bond coats after oxidation for 10 h at 1150 °C. The approximate position of the alumina-alloy interface is indicated by the shaded region. Note that the oxide thickness is several times higher on the grit-blasted sample.

alkali and alkaline-earth metals that have comparable ionization efficiencies.[9] Nevertheless, a more accurate assessment of the impurity concentration in alumina is not possible at this time because of the lack of suitable standards.

While the concentration of impurities in the scale is obviously much higher on the grit-blasted surface of sample B, some of them (Li, Na, Mg, K, and Ca) exhibit qualitatively similar profiles in both samples. The others (Ti and Sr) have dissimilar profiles. Because the two scales have different thicknesses, a better comparison can be made using the normalized oxide thickness (h/h_{ox}), where $h/h_{ox} = 0$ corresponds to the oxide surface. As an example, Figure 8 shows the distributions of Ca and Ti. The profiles of Ca are qualitatively similar (with about a 10 to 30 times higher concentration in the scale on the grit-blasted sample), whereas the profiles of Ti are remarkably different. On sample A, the scale is depleted with Ti (relative to the bulk content), while it is enriched with Ti on sample B.

Thus, in addition to the difference in oxidation kinetics (Figure 3), the α-Al_2O_3 scale growing on the grit-blasted surface has a higher content of various impurities than that formed on the as-aluminized surface. The following section shows that the two oxides also have notably different microstructures.

C. *Microstructural Observations*

The morphology of the alpha-alumina scale growing on the β-(Ni,Pt)Al bond coat is rather complex, both in the as-aluminized condition and after grit blasting. Since the emphasis of this study is on the effect produced by grit blasting, some features of the scale microstructure, although

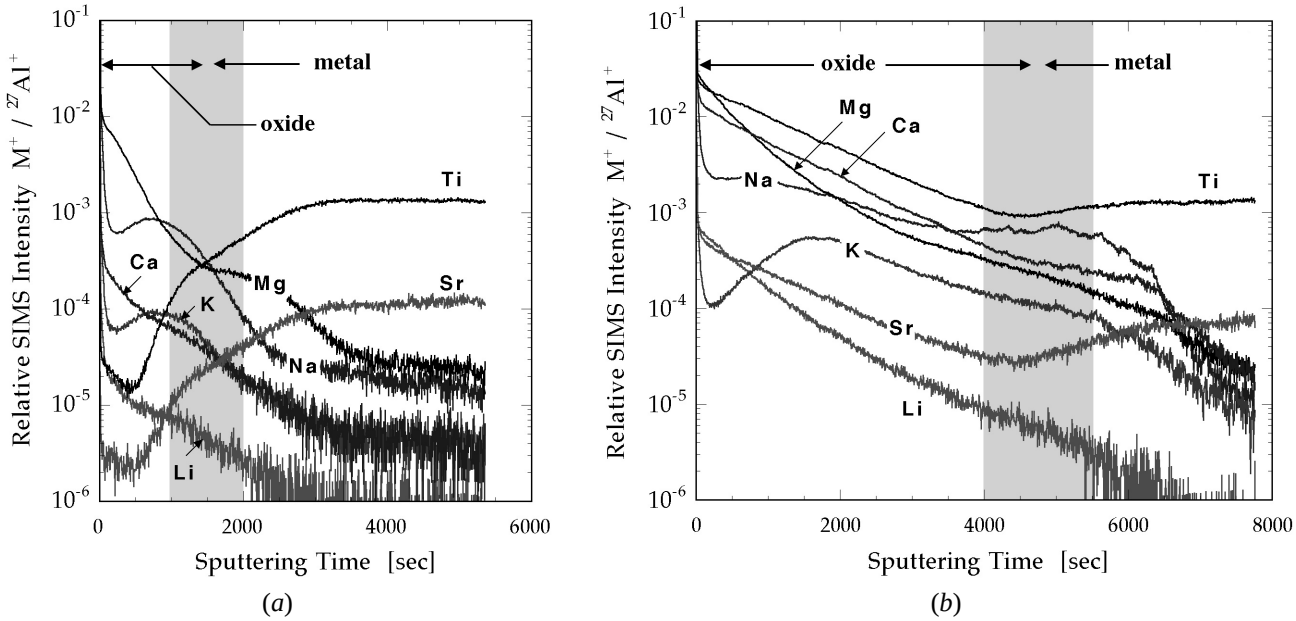

Fig. 7—Relative SIMS intensities, $M^+/^{27}Al^+$ (where $M^+ = {}^7Li^+$, ${}^{23}Na^+$, ${}^{24}Mg^+$, ${}^{39}K^+$, ${}^{40}Ca^+$, ${}^{48}Ti^+$, and ${}^{88}Sr^+$), calculated from the raw data in Fig. 6, showing the impurity distribution in the (*a*) as-aluminized and (*b*) grit-blasted samples. The approximate position of the alumina-alloy interface is indicated by the shaded region.

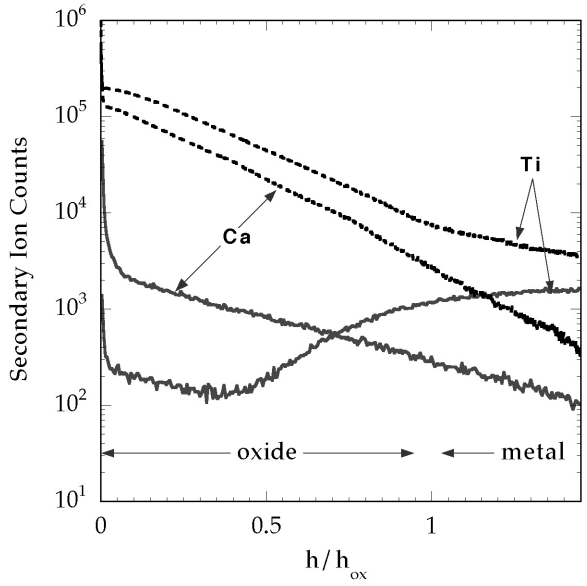

Fig. 8—Comparison between depth profiles of Ti and Ca through alumina scale on the as-aluminized (solid curves) and grit-blasted (dashed curves) samples. The ion counts are plotted as a function of the normalized oxide thickness, h/h_{ox}.

revealing a rich phenomenology, are not considered in this contribution.

Figure 9 shows SEM micrographs of the oxide surface after oxidation for 10 hours at 1150 °C on the two samples analyzed by SIMS. On the as-aluminized sample (Figures 9(a) and (c)), the scale is composed of alumina grains in the form of thin plates outlined by oxide ridges. The lateral size of the grains varies from place to place, being typically smaller along the ridges on the coating surface and larger (up to 10 μm) between the ridges, as shown in Figure 9(a). On the grit-blasted sample (Figures 9(b) and (d)), the oxide surface appears porous and fine-grained, with small inclusions (indicated in Figure 9(d)) of different shape and composition. A typical EDS spectrum of one of these inclusions, shown in Figure 10, demonstrates that it is an alumina-based oxide containing small amounts of Ca, Mg, Ti, and Sr (but not individual phases of impurity oxides). No such foreign oxide phases were found on the as-aluminized sample. The scales were adherent after one 10-hour oxidation cycle on both samples, and no spallation or cracking was observed.

With an increasing number of cycles, a drastic difference in oxidation behavior emerges. Figure 11 shows two series of low-magnification SEM micrographs of the oxide surface on the as-aluminized and grit-blasted samples. After one cycle (Figures 11(a) and (b)), the ridges along the coating grain boundaries are clearly seen. After 13 cycles (Figures 11(c) and (d)), cracking and spalling of the scale occurs on the grit-blasted sample, primarily along the ridges. With further cycling, oxide spallation on the grit-blasted sample becomes rather extensive and, for example, after 72 cycles (Figure 11(f)), the majority of the primary (first-formed) oxide has spalled off. Scale spallation occurs over large areas covering one or several adjacent grains of the bond coat. In contrast, the scale is still intact on the as-aluminized sample (Figure 11(e)), and only a few places were found where it had failed in the course of 72 10-hour cycles.

In agreement with the kinetics data in Figure 3, the oxide thickness is about 3 times smaller on the as-aluminized sample (Figure 12). The fracture cross section of a thin alumina layer after oxidation for 720 hours (72 10-hour cycles) of the as-aluminized bond coat is presented in Figure 12(a). For comparison, Figure 12(b) shows a 6- to 7-μm-thick alumina scale formed on sample B after the same oxidation time. The microstructure of the fracture section indicates that this is a portion of the originally formed oxide which has failed in the last cooling cycle. A more typical example of the oxide failure on the grit-blasted sample is

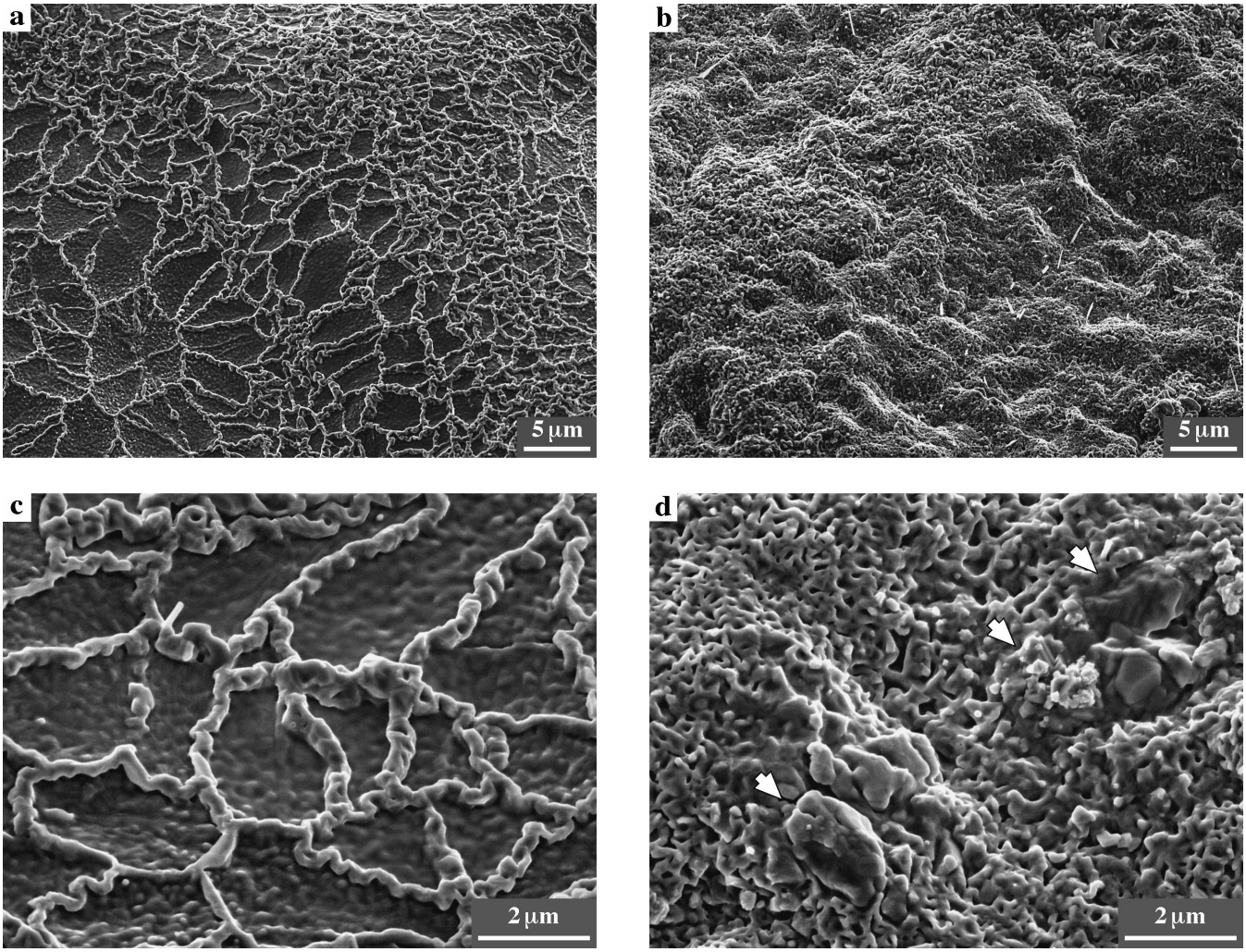

Fig. 9—Microstructure of the alumina surface after oxidation for 10 h at 1150 °C of the (*a*) and (*c*) as-aluminized and (*b*) and (*d*) grit-blasted samples. Foreign oxide inclusions are indicated by the arrows in (d).

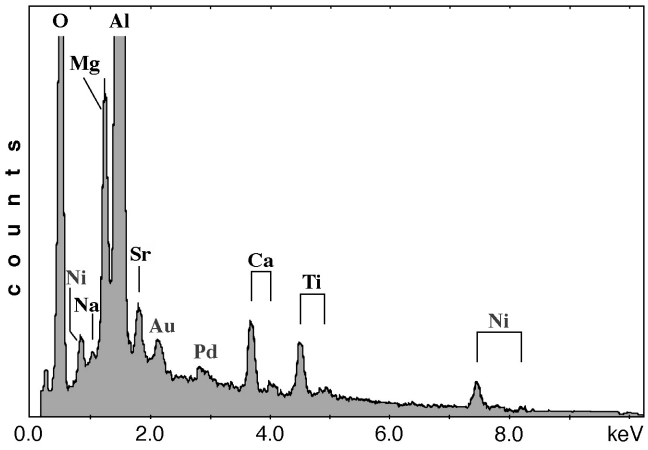

Fig. 10—Typical EDS spectrum from an oxide inclusion on the scale surface after oxidation of the grit-blasted bond coat. The peaks of Au and Pd are from a thin conductive coating on the sample surface. Some part of the Ni signal may appear from the alloy substrate.

presented in Figure 13(b), where a number of alumina layers, repeatedly formed and spalled during cyclic oxidation, can be seen. On the as-aluminized sample, some local cracking of the scale occurs along grain-boundary ridges, as shown in Figure 13(a).

The polished cross sections of the bond coat after 100 10-hour cycles (1000 hours total exposure at 1150 °C) in Figures 14 and 15 illustrate the difference in coating microstructures between samples A and B. On the as-aluminized sample (Figure 14), the alumina scale is mainly intact and exhibits thickness variations in the range from 1 to 5 μm. During high-temperature exposure, the aluminum content in the bond coat decreases due to oxidation and interdiffusion with the superalloy. Based on the EDS results, after 1000 hours at 1150 °C, the bond coat consists of γ' phase (nominally γ'-Ni_3Al with about 20 at. pct Al, also containing Cr, Co, Pt, and refractory metals) and a discontinuous zone of β phase (with 31 to 32 at. pct Al) remaining under the scale. Because the growth rate of the scale is very low (Figure 3) and virtually no spallation occurs on the as-aluminized bond coat, aluminum depletion due to interdiffusion is predominant in the present conditions. The γ' phase does not show any contrast on the cross section, whereas the β phase is clearly seen after etching, as indicated in Figure 14.

As a result of repeated scale spallation on the grit-blasted

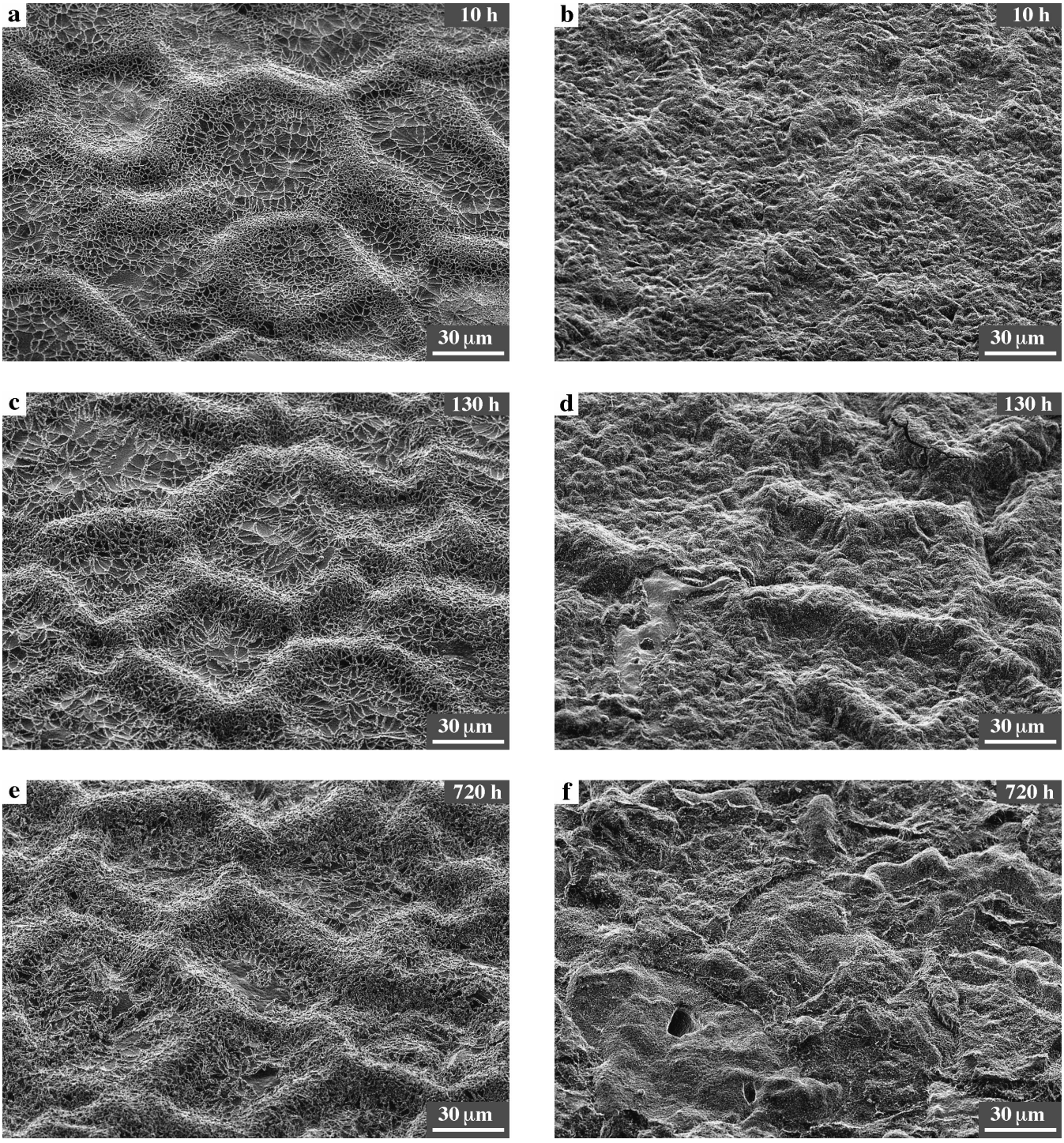

Fig. 11—Evolution of the scale morphology during cyclic oxidation at 1150 °C (10-h cycles) on the (*a*), (*c*), and (*e*) as-aluminized and (*b*), (*d*), and (*f*) grit-blasted samples. All SEM micrographs were taken at the same magnification after (*a*) and (*b*) 10 h, (*c*) and (*d*) 130 h, and (*e*) and (*f*) 720 h.

sample, only small portions of the oxide appear intact after cross sectioning (Figure 15). The higher oxidation rate and spallation produce a more substantial Al depletion; therefore, the aluminum-rich β phase disappears after about 400 hours. The EDS analysis and etched microstructure in Figure 15 indicate that, after 1000 hours at 1150 °C, the bond coat consists of γ' and another low-Al phase (marked as γ in Figure 15), which contains, on average, about 12 at. pct Al and 16 at. pct Cr. (It is likely that this phase is actually a mixture of two different phases with higher and lower Cr contents; however, their size is too small for the EDS analysis. Note also that, in the presence of several other elements in the bond coat, the phase equilibria of the ternary Ni-Cr-Al diagram may not be adequate, so the designation "γ" is used for simplicity).

Another distinctive feature of the grit-blasted sample is

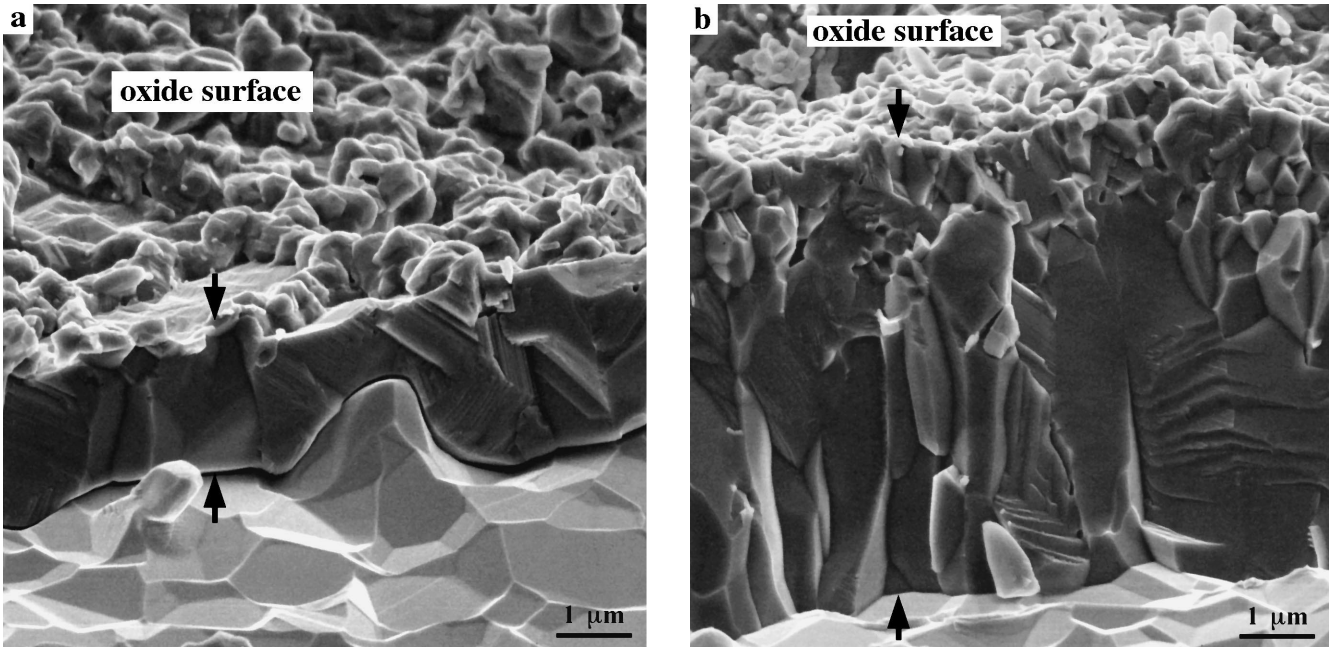

Fig. 12—Fracture cross sections of the alumina scales formed on the (*a*) as-aluminized and (*b*) grit-blasted samples after oxidation for 720 h (72 ten-hour cycles) at 1150 °C. The arrows indicate the oxide surface and the oxide-metal interface.

the formation of large internal cavities in the bond coat (Figure 15(a)). As discussed previously,[11] this type of coating degradation is likely to be related to the volume reduction in the bond coat as a result of aluminum depletion and phase transformation from β to γ' and then to γ. Therefore, internal cavitation is more pronounced when Al consumption is faster. Correspondingly, fewer cavities (after the same 1000-hour exposure) were observed on the as-aluminized sample due to its low oxidation rate and, hence, slower Al depletion.

IV. DISCUSSION

The α-Al_2O_3 scale formed on the surface of the platinum-modified nickel-aluminide bond coat exhibits excellent spallation resistance and a very low growth rate during cyclic oxidation at 1150 °C, in agreement with other studies.[1,4,5,12] In fact, the rate of oxidation of the β-(Ni,Pt)Al bond coat is even smaller than that of the most-oxidation-resistant Fe-Cr-Al alloys, such as Kanthal APM (Kanthal International, Hallstahammar, Sweden) or Inco MA956 (INCO Limited, Toronto, Ontario, Canada). However, as the results of this work show, these superior properties are only characteristic of the bond coat in the as-aluminized condition. Meanwhile, in practical applications, the coating surface is usually grit-blasted prior to TBC deposition. Comparing the oxidation kinetics and spallation resistance (Figures 3 and 11 through 13), it appears that the performance of the grit-blasted samples is much poorer, at least at 1150 °C. It can be concluded, therefore, that grit blasting of the bond-coat surface has an adverse effect on the oxidation behavior. Summarizing the results presented previously, the effect of grit blasting can be described as follows.

(1) *Grit blasting introduces impurities into the bond-coat surface*. A substantial enrichment of various impurities, in particular, alkali, alkaline-earth elements, and titanium, was detected by SIMS not only at the grit-blasted surface but also deeper into the subsurface layer (Figure 4(b)). The most important source of impurities appears to be the blasting media. The SIMS analysis of the alumina particles used for grit blasting confirms the presence of all the impurities on their surface (unpublished study). Thus, these elements are transferred from the corundum particles to the bond-coat surface. Most likely, the impurities are trapped in small surface cracks and fissures, created by the impact of high-speed particles, and embedded into the coating by plastic deformation of the surface layer during grit blasting. For this reason, the surface contamination, produced by grit blasting, cannot be easily removed by standard cleaning procedures. An increased impurity content (relative to the bulk coating) on the as-aluminized surface (Figure 4(a)) indicates that some part of the surface contamination may be introduced during sample handling or may be due to adsorption from the ambient atmosphere. Nevertheless, the concentration of impurities on the as-aluminized bond-coat surface is far smaller than after grit blasting.

(2) *The impurities become incorporated into the growing alumina scale during oxidation*. Although the major oxide phase formed on the bond-coat surface at 1150 °C is α-Al_2O_3, all the alkali and alkaline-earth metals, which have a very high affinity with oxygen, also form oxides and become incorporated into the alpha-alumina grains. Apparently, in some locations, their concentration can exceed the solubility limit in alpha-alumina, since the impurities also precipitate as mixed oxides detected on the scale surface (Figure 10). The impurity cations, such as Na^+ or Ca^{2+}, are also expected to segregate at the alumina grain boundaries on account of their large ionic radii and limited solubility in α-Al_2O_3. One possible consequence is that these impurities may affect

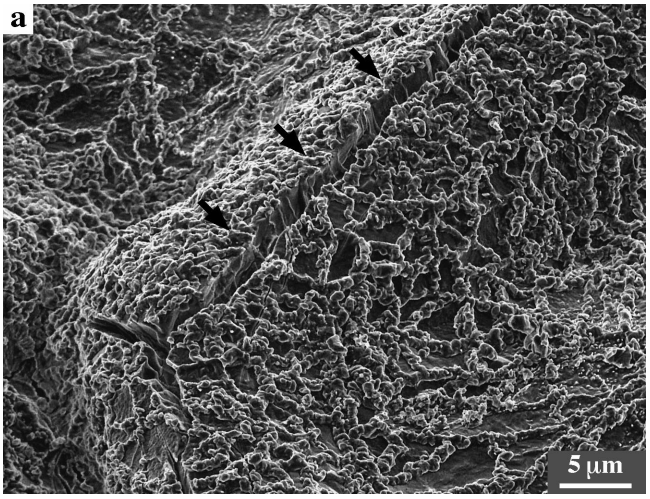

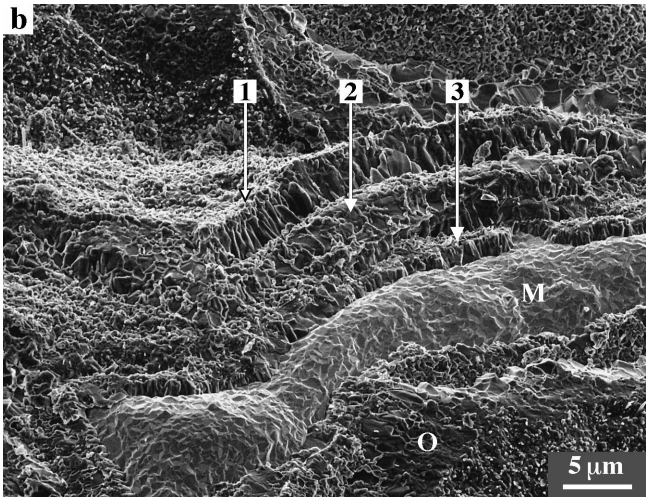

Fig. 13—Typical failure of the scale after oxidation for 720 h (72 ten-hour cycles) at 1150 °C. (*a*) Cracking along grain boundary ridges on the as-aluminized bond coat (the crack is indicated by the arrows). (*b*) Multiple spalling of the scale on the grit-blasted bond coat. Three distinct oxide layers are apparent and are marked in the order of their formation from 1 to 3; the next oxidation cycle will produce one more alumina layer on the exposed metal surface (M).

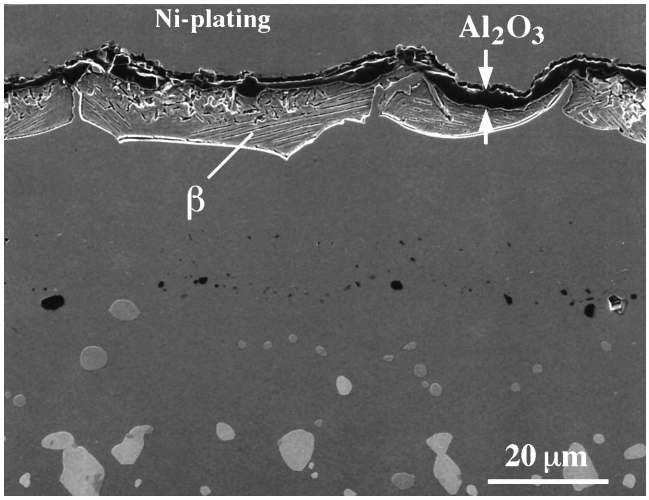

Fig. 14—Cross section of the as-aluminized bond coat after oxidation for 1000 h (100 ten-hour cycles) at 1150 °C. The β-(Ni,Pt)Al phase, revealed by etching, and thin alumina scale are indicated. The major phase in the coating is γ'-Ni_3Al.

the diffusivity of oxygen and aluminum in the growing scale.

(3) *The scale containing impurities has a significantly higher growth rate* than the nominally pure alumina scale on the as-aluminized bond coat of the same bulk composition. Although the effect of these individual impurities on oxidation is not known, the results show that the scale containing a higher concentration of impurities grows faster. The ten-fold increase of the oxidation rate constant and significant changes in oxide morphology are believed to be due to the presence of alkali and alkaline-earth elements in the alumina scale. This is consistent with recent observations of the adverse effect of Na and Ca on the alumina morphology and spalling resistance of Fe-Cr-Al alloys.[13] Other impurities (for example, Ti, Si, Fe or the anions Cl and P) may contribute as well.

Another feature associated with the incorporation of impurities on the oxidation behavior is the scale morphology, particularly, the grain size. If the oxide growth is controlled by grain-boundary diffusion (which is commonly accepted in the case of alumina[14]), then the scale with larger grains should have a smaller growth rate. Indeed, on the as-aluminized bond coat, the average in-plane size of alumina grains is quite large (2 to 3 μm) and does not increase significantly with oxidation time. In contrast, the grains are much smaller on the grit-blasted surface, especially at the beginning of oxidation. Most probably, this is a result of impurities and various surface defects, which facilitate nucleation of the α-Al_2O_3 oxide.

The higher oxidation rate of the grit-blasted surface results in a thicker alumina layer. This has a number of negative consequences. One of them is aluminum depletion of the bond coat. The EDS analysis shows that the β-(Ni,Pt)Al phase on the grit-blasted sample transforms completely into γ'-Ni_3Al after about 400 hours at 1150 °C. Subsequent Al depletion leads to precipitation of the nickel-based solid-solution phase. Repeated spallation of the thick oxide and reoxidation of the exposed metal further accelerates aluminum depletion. Although the formation of spinel phases was not observed during the oxidation time studied, it is clear that such nonprotective oxides will eventually appear at a low residual Al concentration in the bond coat. In contrast, the more slowly growing scale on the as-aluminized surface depletes less aluminum from the bond coat, and so the β-(Ni,Pt)Al phase remains present after oxidation for 1000 hours. (Obviously, the reduction of Al concentration due to interdiffusion with the superalloy is nearly the same in both samples).

Another negative consequence of the higher oxidation rate of the grit-blasted sample is the coating degradation by the formation of internal cavities (Figure 15(a)). This process is also considered to be caused by aluminum depletion of the bond coat.[11]

(4) Perhaps the most dramatic consequence of the high oxidation rate is *the poor spallation resistance of the alumina layer.* Spallation from the grit-blasted bond coat starts as early as after ten 10-hour cycles and becomes

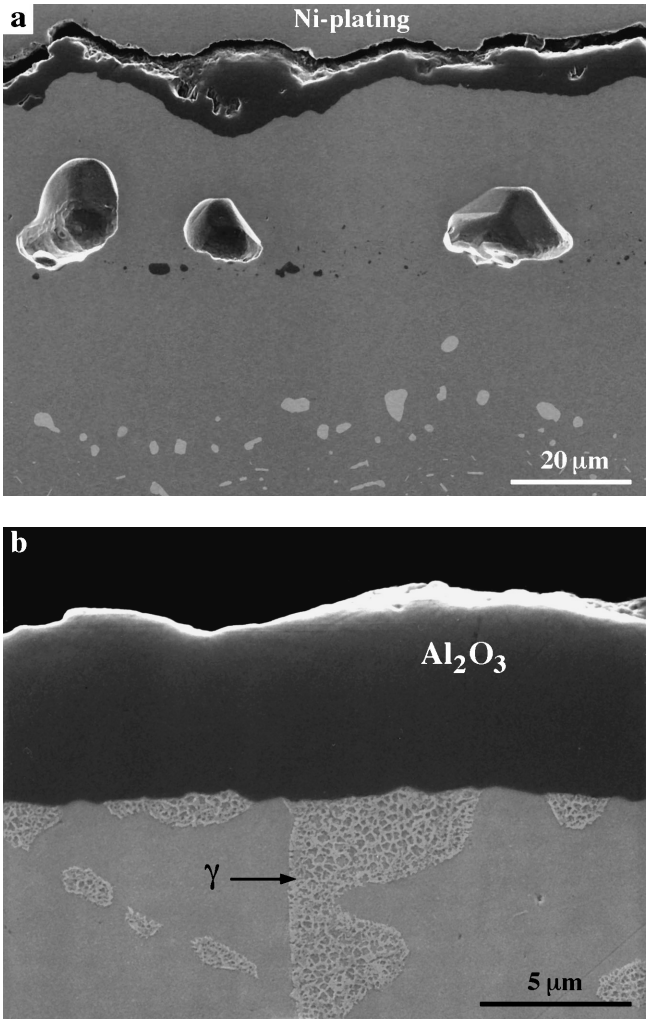

Fig. 15—Cross section of the grit-blasted bond coat after oxidation for 1000 h (100 ten-hour cycles) at 1150 °C showing (*a*) large internal cavities in the bond coat and alumina layer remaining after multiple failure; and (*b*) precipitation of a low-aluminum phase, revealed by etching (presumably, the solid solution γ-phase), in the γ'-Ni_3Al matrix.

very extensive after 30 cycles, whereas on the as-aluminized sample, spallation is insignificant even after 100 cycles (1000 hours at 1150 °C). This difference is rather vividly illustrated in Figure 16, which shows a sample, one side of which was grit-blasted before oxidation and the other side was masked. The low-magnification optical and SEM images of the sample after cyclic oxidation at 1150 °C (Figures 16(b) and (c)) demonstrate extensive spallation on the grit-blasted side and essentially intact scale on the as-aluminized side.

In the oxidation literature, spallation is usually attributed to sulfur segregation to the oxide-metal interface. Since the as-aluminized and grit-blasted samples apparently contain equal amounts of sulfur in the coating, the difference in spallation behavior cannot be ascribed to sulfur. One possible explanation for the increased propensity for oxide failure by spallation on the grit-blasted surfaces is that impurities, introduced by grit blasting prior to oxidation, segregate to the oxide-metal interface and lower its fracture resistance in much the same way as is generally accepted for sulfur. It is not known, however, if the impurities detected in this

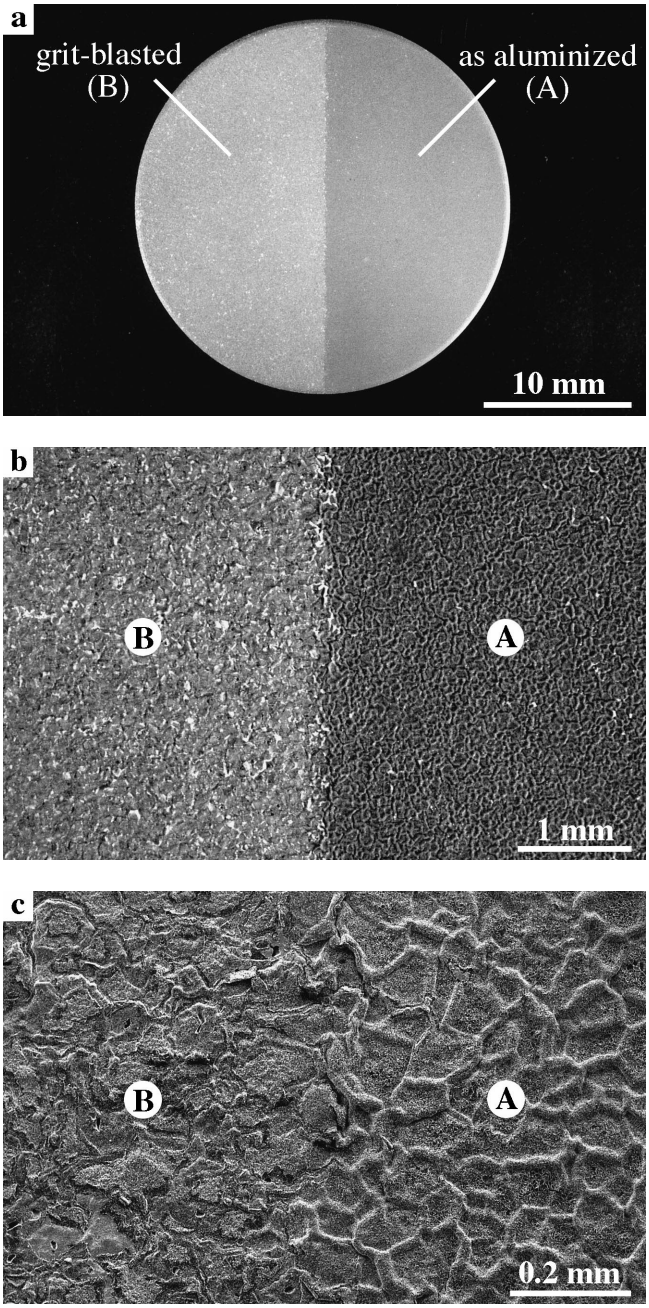

Fig. 16—(*a*) General view of the sample that was grit blasted prior to oxidation on one side only (the other side was masked) after 72 ten-hour cycles at 1150 °C. The (*b*) optical and (*c*) SEM micrographs show the area near the boundary between the (A) as-aluminized and (B) grit-blasted sides. Oxide spallation occurs on side B, whereas the scale is intact on side A.

work have a direct effect on the interface fracture resistance. Besides, none of the analyzed impurities showed a local maximum near the oxide-metal interface on the SIMS depth profiles (Figure 6), and, moreover, the concentration of impurities near the interface is about the same on both samples. Therefore, it seems unlikely that the difference in spallation resistance between the grit-blasted and as-aluminized bond coats is directly associated with impurity segregation.

The other explanation is a mechanical one. Cooling from the oxidation temperature during thermal cycling induces a large compressive stress in the scale as a result of its thermal-expansion mismatch with the superalloy. The thicker the

oxide, the higher the strain energy in the oxide and, hence, the larger the driving force for failure on cooling. From the oxidation kinetics of the grit-blasted sample in Figure 3, it can be concluded that extensive spallation starts when the oxide thickness reaches approximately 5 μm (a mass gain of about 0.9 mg/cm^2). This value can be considered to be a "critical" oxide thickness, and the corresponding time to failure for the grit-blasted sample is around 300 hours at 1150 °C. Extrapolating the data for the as-aluminized sample, such a thickness will be attained after nearly 3000 hours without grit blasting.

Another aspect that can affect the spallation behavior is the configuration of the oxide-metal interface. During cooling from the oxidation temperature, tensile stresses develop at the convex areas normal to the interface[15,16] and may lead to interface separation and initiate local failure.[17,18] For this reason, cracking and spallation of the scale first occurs along grain-boundary ridges on the grit-blasted surface, as shown in Figure 11(d). During further cycling, the initial roughness increases as a result of repeated oxide spallation and reoxidation. In addition, the roughness is enhanced by plastic deformation (surface rumpling) of the bond coat.[11] Although surface roughness also increases on the as-aluminized sample (grain-boundary ridges become higher or valleys deepen), the scale remains mainly intact. The critical difference is the oxide thickness. When it is small compared with the radius of curvature of interface undulations, the normal stresses at asperities are also small,[15,16–18] and the oxide remains in contact with the alloy. After prolonged oxidation, when the oxide becomes thick enough, scale cracking occurs along ridges on the as-aluminized bond coat (Figure 13(a)).

As mentioned in the Introduction, the impurity content may vary depending on the grit-blasting media used in each case. Perhaps, less contamination may be expected if ultra-high-purity corundum particles were used. However, such a powder may be too costly for industrial applications, especially since recycling of the powder will invariably lead to gradual accumulation of various impurities from blasting equipment on the surface of particles.

Finally, although the focus of this study has been on the oxidation behavior of (Ni,Pt)Al bond coats, the findings are of significance for the life of TBCs, in particular, the electron-beam physical vapor deposition YSZ coatings. Some attempts have recently been made to correlate TBC life with the thickness of the alumina layer formed beneath the TBC.[19] Based on the results of this work (and assuming that the oxidation behavior of the TBC-coated material is not different from that of the bare bond coat), the life of the TBC deposited on the grit-blasted surface is expected to be far shorter than without grit-blasting. Thus, any life prediction model should consider not only the basic coating parameters and testing conditions but also the details of surface treatment prior to TBC deposition and its effect on oxidation kinetics, oxide microstructure, and susceptibility to spalling.

V. CONCLUSIONS

1. Grit blasting of the (Ni,Pt)Al bond-coat surface leads to contamination by various impurities, in particular, the alkali and alkaline-earth elements (Li, Na, K, Mg, Ca, and Sr) and titanium in the grit-blasting media.
2. During subsequent high-temperature oxidation, the impurities become incorporated into the growing α-Al_2O_3 scale and significantly accelerate oxide growth. The effect on the alumina growth rate is presumably caused by their influence on oxygen and/or aluminum diffusivity through the scale.
3. The high growth rate of alumina, combined with roughening (rumpling) of the bond-coat surface during cyclic oxidation, result in cracking and spalling of the scale followed by a mass decrease after only 30 10-hour cycles at 1150 °C.
4. The α-Al_2O_3 scale formed on the as-aluminized surface (without grit blasting) has a much lower impurity content and a slower growth rate, as well as an excellent spalling resistance during cyclic oxidation.
5. The results of this work suggest that impurities introduced by grit blasting of the bond-coat surface prior to TBC deposition are expected to have a strong detrimental effect on TBC durability.

ACKNOWLEDGMENTS

The authors are grateful to Dr. T. Mates (UCSB, Santa Barbara, CA) for conducting SIMS depth profiling. The research was supported by the Advanced Gas Turbine Systems Research (AGTSR) program through the Department of Energy.

REFERENCES

1. B.M. Warnes and D.C. Punola: *Surface Coating Technol.*, 1997, vol. 94–95, pp. 1-6.
2. M. Gell, K. Vaidyanathan, B. Barber, J. Cheng, and E. Jordan: *Metall. Mater. Trans. A*, 1999, vol. 30A, pp. 427-35.
3. W.Y. Lee, Y. Zhang, I.G. Wright, B.A. Pint, and P.K. Liaw: *Metall. Mater. Trans. A*, 1998, vol. 29A, pp. 833-41.
4. B.A. Pint, I.G. Wright, W.Y. Lee, Y. Zhang, K. Prüssner, and K.B. Alexander: *Mater. Sci. Eng. A*, 1998, vol. A245, pp. 201-11.
5. Y. Zhang, W.Y. Lee, J.A. Haynes, I.G. Wright, B.A. Pint, K.M. Cooley, and P.K. Liaw: *Metall. Mater. Trans. A*, 1999, vol. 30A, pp. 2679-87.
6. J.L. Smialek and B.K. Tubbs: *Metall. Mater. Trans. A*, 1995, vol. 26A, pp. 427-36.
7. G.H. Meier, F.S. Pettit, and J.L. Smialek: *Mater. Corr.*, 1995, vol. 46, pp. 232-40.
8. D. Monceau, K. Bouhanek, R. Peraldi, A. Malie, and B. Pieraggi: *J. Mater. Res.*, 2000, vol. 15, pp. 665-75.
9. R.G. Wilson, F.A. Stevie, and C.W. Magee: *Secondary Ion Mass Spectrometry: a Practical Handbook for Depth Profiling and Bulk Impurity Analysis*, John Wiley, New York, NY, 1989.
10. M. Textor: in *Secondary Ion Mass Spectrometry, SIMS III*, A. Benninghoven *et al.*, eds., Springer-Verlag, Berlin, New York, 1982, pp. 372-76.
11. V.K. Tolpygo and D.R. Clarke: *Acta Mater.*, 2000, vol. 48, pp. 3283-93.
12. V.K. Tolpygo and D.R. Clarke: *Mater. High Temp.*, 2000, vol. 17, pp. 59-70.
13. V.K. Tolpygo and H.J. Grabke: *Scripta Mater.*, 1998, vol. 38, pp. 123-29.
14. M. LeGall, A.M. Huntz, B. Lesage, C. Monty, and J. Bernardini: *J. Mater. Sci.*, 1995, vol. 30, pp. 201-11.
15. C.H. Hsueh and A.G. Evans: *J. Appl. Phys.*, 1983, vol. 54, pp. 6672-86.
16. X.Y. Gong and D.R. Clarke: *Oxid. Met.*, 1998, vol. 50, pp. 355-76.
17. V.K. Tolpygo and D.R. Clarke: *Acta Mater.*, 1998, vol. 46, pp. 5167-74.
18. D.R. Clarke and W. Pompe: *Acta Mater.*, 1999, vol. 47, pp. 1749-56.
19. M.J. Stiger, N.M. Yanar, M.G. Topping, F.S. Pettit, and G.H. Meier: *Z. Metallkd.*, 1999, vol. 90, pp. 1069-78.